ACS OMEGA

Open Access

http://pubs.acs.org/journal/acsodf

Article

Effect of Red Mud and Rice Husk Ash-Based Geopolymer Composites on the Adsorption of Methylene Blue Dye in Aqueous Solution for Wastewater Treatment

Khoa Dang Nguyen,* Trang Tran Thu, Anh Thi Hoang Tran, Oanh Thi Kim Le, Suresh Sagadevan, and Noor Haida Mohd Kaus*

Cite This: *ACS Omega* 2023, 8, 41258−41272

Read Online

ACCESS | Metrics & More | Article Recommendations

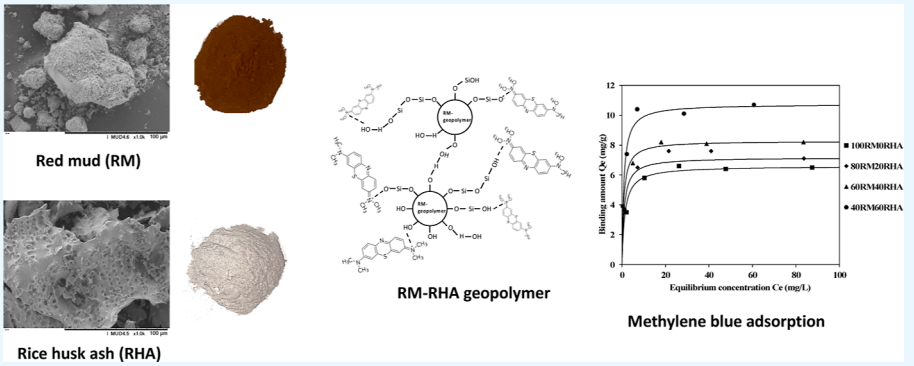

ABSTRACT: In this study, geopolymer originating from locally industrial byproducts as red mud (RM) was successfully prepared in the presence of different loadings of rice husk ash (RHA) used for the adsorption of methylene blue (MB) in wastewater. During geopolymerization, various mixing amounts between RM and RHA were conducted when the weight ratio of binder solution/activated alkali-metal solution (Na_2SiO_3/ NaOH 7 M) was 2.5 and the curing temperature was set at 60 °C for 24 h. As a result, the surface area value of the prepared geopolymer composited with RHA at 0 and 60% was increased from 19.2 to 29.5 m^2/g, while the BJH pore size of the prepared geopolymer was reduced to 6.68 and 5.76 nm, respectively. In the dye removal test, higher additions of RHA in the RM-geopolymer maintained better retention of the MB ion due to the increase in the adsorption binding site. The maximum uptake amount of dyes performed at pH 8 was changed from 6.59 to 10.74 mg/g, while RHA was from 0 to 60% after 180 min of immersion in MB solution. The adsorption isotherms well obeyed the Langmuir model, as the relative coefficient R^2 was 0.999. Based on these, the initial agricultural waste as RHA and industrial byproducts as RM were valued as functional materials used for dye treatment in wastewater.

1. INTRODUCTION

The textile industry is widely developed globally and employs workers around the world. Despite its indisputable contributions, this industry is one of the largest polluters, consuming high amounts of fuels and chemicals.[1] The damage to the environment caused by the textile industry is mainly due to untreated wastewater being discharged directly into the aquatic environment. Synthetic dyes are not only unsightly but also interfere with the passage of light through the water, thereby reducing the rate of photosynthesis, reducing dissolved oxygen levels, affecting the entire aquatic ecosystem, and harming the organisms in contact with them.[2] Textile dyes are also considered to be toxic, mutagenic, and carcinogenic agents that exist as environmental contaminants and through the food chains providing bioanalytical processes; therefore, higher levels of contamination are present in organisms at higher trophic levels.[3] It is well known that water-soluble azo dyes are less susceptible to oxidative catabolism due to their high chrominance and cause serious environmental pollution due to their electron deficiency. Therefore, wastewater from the textile industry is often difficult to decompose.[4] Various classifications of dyes based on the charge of the chromophore group dissolved in water, such as cationic dyes, anionic dyes, and nonionic dyes (water-insoluble), are considered to be the three common dye groups.[5] In particular, due to its high water

Received: July 1, 2023
Accepted: September 27, 2023
Published: October 24, 2023

solubility and color fastness, in the dyeing and ink manufacturing industries, methylene blue (MB) (Figure 1) is

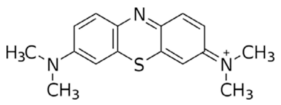

Figure 1. Chemical structures of MB.

a cationic dye that has been most widely used and more toxic than anionic ones,[6,7] which are found in industrial wastewater anywhere in the world and can be released into the aquatic environment easily. Residual dyes in wastewater when they are released into water, even at low concentrations, will not only cause sensory loss due to noticeable and undesirable colors but can also have adverse health effects on aquatic organisms and human beings.[8,9] Dye removal from wastewater by adsorption is a method of current interest because of its high simplicity, environmental friendliness, low cost, and potential efficiency. The use of new adsorbents to remove organic and inorganic pollutants from wastewater has been intensively synthesized and thoroughly investigated in recent years,[10] with the aim of finding a desirable adsorption material recovered from industrial wastes or byproducts to absorb hazardous substances from wastewater.[11−13]

Geopolymers are inorganic polymers and a new synthetic material from alumina-silicate involving the chemical reaction between aluminum-silicate oxides and alkali metal silicate solutions under highly alkaline conditions.[14] Depending on the ratio of Si/Al, the geopolymers are classified into three types of three-dimensional network structures, such as polysialate (−O−Si−O−Al−O−), polysialate siloxo (−O−Si−O−Al−O−Si−O−), and polysialate disiloxo (O−Si−O−Al−O−Si−O−Si−O−). As seen, the initial Si/Al ratio in the starting material could be the decisive factor in terms of the mechanical strength of the conducted geopolymer, which typically ranges from 3.0 to 3.8.[15,16] Preparation and characterization of geopolymers with different synthesis conditions and adsorption applications have been carried out in many studies.[17−22] Usually, initial materials with high SiO_2 and Al_2O_3 content are favored for the geopolymerization.[23] During the formation process, in the presence of the materials, active substances such as high concentrations of alkali-metal solutions and binders such as sodium silicate (e.g., Na_2SiO_3) would be added to the mixture.[14] This binder has the role of increasing the amount of silica in the paste and supporting the formation of Si−O−Si bonds, creating a larger area than the other bonds in the geopolymer structures. Therefore, the properties of the resulting geopolymers could be improved. The type of alkali solution with wide-range concentrations, the temperature curing, the storage duration, and especially the ratio between the alkali solution and the binder have been identified as having a significant influence on the properties of the prepared geopolymer in many researches. It has been reported that the geopolymer activated with NaOH was determined to give higher compressive strength than solutions containing KOH at the same concentration,[24] where the recommended alkali solution concentration ranges from 5 to 15 M.[25] It is possible to optimize the bonding regeneration in the polymeric structure of the geopolymer by increasing the concentration of an alkali activator, which in turn can enhance the solubility of silicate and alumino compounds in the raw material.[16] In addition, due to hydration and shrinkage, the strength is able to be decreased after curing at temperatures above 80 °C owing to the disruption in the geopolymer structure.[26] The geopolymer process was most efficient at temperatures between 60 and 80 °C,[27] and the mass ratio of Na_2SiO_3/NaOH was about 2.5.[28]

The consumption of bauxite for the extraction of aluminum increased by 30% in 2019 when compared to the year 2018 at the same time. Approximately 73% of bauxite is refined by the Bayer process. It has been reported that about 4−5 tons of red mud (RM), the main byproduct for extracting alumina from bauxite ore, is discarded per 1 ton of aluminum metal produces.[29,30] In general, the mud produced is usually transported to a dam, and in sequence, it can go through a dehydration and drying process to reduce its volume and maintenance costs.[31,32] The disposal of RM poses significant environmental concerns, especially if handled on land or in bodies of water. Also, the use of sodium hydroxide in the extraction of alumina, which is highly alkaline in nature (pH value from 10.0 to 12.5), causes considerable impacts on aquatic ecosystems and is identified as a hazardous waste.[33] Bauxite has a very diverse mineral composition depending on the sources and technical process parameters, including gibbsite, hematite, boehmite, kaolinite, anatase, rutile, and quartz.[34] The chemical compositions of RM included many oxides, such as SiO_2, Al_2O_3, Fe_2O_3, and CaO, with different distribution percentages, mainly depending on the bauxite ore type and the different alumina production processes.[35] Therefore, RM is strongly considered to be used to produce geopolymer[35,36] due to the fact that the remaining caustic in the RM did not require neutralizing by acid, which was an advantage of this process. However, the SiO_2/Al_2O_3 molar ratio of RM is often much smaller than the range satisfied in the geopolymer formulation.[37−40] Rice husk (RH) is an agricultural waste that can overcome this problem due to its high content of silica oxide (SiO_2) as a potential filler to improve the properties of RM-based geopolymers, such as mechanical properties and contaminant adsorption capacity. RH is one of the main biomass byproducts after the rice milling process. Silica, with small amounts of inorganic compounds, is the major constituent of RH. With a composition of about 80−98% silica after complete combustion, rice husk ash (RHA), derived from RH combustion, is one of the most silica-rich raw materials. It is highly porous and light and has a very large external surface area, which has been used effectively. The amount and silica phase of RHA that were modified after pyrolysis and pretreatment under different conditions have been explored in several reports.[41−43] Moreover, the use of silica oxide as an adsorbent porous material has received much attention in the water purification process.[44−47] However, studies on the preparation of geopolymers from RM and RHA have mainly focused on the mechanical properties and pretreatment of the starting materials[48−51] or catalyst delivery system.[52] Therefore, the aim of this study is to systematically investigate the effect of loading amounts of RHA on the formation and related properties of the RM-based geopolymer used for improving the simulating adsorption of MB in wastewater. In order to carry out interactions between RM and RHA in the geopolymer compositions, Fourier transform infrared spectroscopy (FT-IR) was performed. Meanwhile, X-ray diffractometers (XRD) and X-ray fluorescence (XRF), as well as scanning electron microscopy−energy dispersive X-ray spectroscopy (SEM−EDS), were tested to determine the element phase and

https://doi.org/10.1021/acsomega.3c04691
ACS Omega 2023, 8, 41258−41272

distribution in the mixed geopolymer samples. Prior to the dye adsorption test, the Brunauer–Emmett–Teller (BET) surface area, the Barrett–Joyner–Halenda (BJH) pore size distribution, and Zeta potential were evaluated to predict the adsorption tendency of the geopolymer materials.

2. EXPERIMENT

2.1. Materials. RM in this study was locally collected from Lam Dong Province, Vietnam, while RHA was taken from Long An Province, Vietnam. Other chemicals such as hydrochloride acid (HCl, 36%), sodium hydroxide (NaOH, 99%), sodium silicate (Na_2SiO_3, SiO_2: 28.5%, and Na_2O: 8.5%), and MB were received from Merck, Germany. All chemicals used in the preparation of geopolymer and the adsorption experiment of MB were analytical grade.

2.2. Pretreatment of Red Mud and Rice Husk Ash. As received, RM (Figure 2a) and RHA (Figure 2b) were ground and sieved through a 245 μm sieve, followed by washing in water three times and drying at 105 °C for 24 h. The main components of RM and RHA were determined via XRF measurement (ZSX Primus II; Rigaku Corp., Japan) as presented in Table 1.

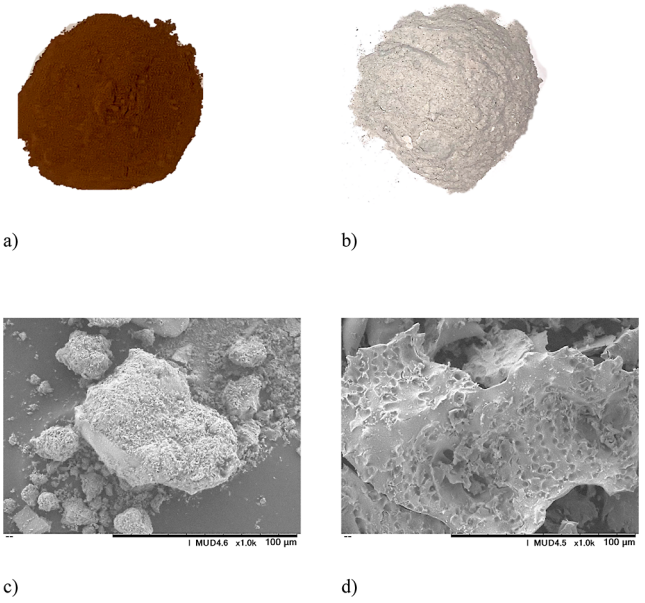

Figure 2. Appearance of RM (a) and RHA (b) and SEM at the magnification of 1000× of RM (c) and RHA (d).

Table 1. Main Chemical Components (Weight %) of RM and RHA

	the main components (weight %)				
samples	SiO_2	Al_2O_3	Fe_2O_3	CaO	TiO_2
RM	6.33	13.44	45.8	3.41	5.84
RHA	90.5	0.46	0.74	0.97	0.04

The SEM images of RM and RHA are also in Figure 2. At a magnification of 1000× (Figure 2c), the morphology of RM was observed at various shapes, and the impurity was somehow seen with different size distributions on the surface of the RM particle at a magnification of 1000×. In the case of RHA (Figure 2d), the porous structure was obtained on the surface of RHA, which agrees with other report.[41]

2.3. Preparation of the Geopolymer. The pretreated RM and RHA were mixed with the appropriate amount in addition to NaOH 7 M and Na_2SiO_3 aqueous solutions. The mass ratio between Na_2SiO_3/NaOH was kept at 2.5. The loading of RHA was varied in the range of 0 to 60% (Table 2). The paste was mixed within 10 min at room temperature before being poured into the cubic-plastic mold (50 × 50 × 50 mm^3) followed by drying at 60 °C for 24 h. After that, the geopolymers were obtained. Before measurements, these samples were ground and sieved through a 245 μm sieve, followed by washing in the excess amount of deionized water until the pH reached a neutral value. For denotes, the samples were named as%RM%RHA. For example, the geopolymer prepared with 100% RM and 0% RHA was 100RM0RHA. The appearance of the geopolymers prepared from RM and RHA is shown in Figure 3.

2.4. Characterization. *2.4.1. Fourier Transform Infrared Spectroscopy.* To confirm the formation of geopolymer and characterize the interaction between RM and RHA in the presence of alkaline activation and silicon binder solution, FT-IR spectra were recorded in a JASCO FT-IR/4100 spectrometer. The dried samples were ground with potassium bromide (KBr) in a portion of 1/10 (wt %) and scanned in the transmittance model. Spectra were taken from 4000 to 400 cm^{-1} wavenumber with a resolution of 2 cm^{-1}.

2.4.2. X-Ray Diffractometer. The functionalization of RM, RHA, and geopolymers such as the crystalline and amorphous forms was observed by XRD (Smart Lab, Rigaku, Japan) with Cu K_a radiation (λ = 1.54056 Å) at 40 kV and 30 mA. The XRD patterns were taken in the 2θ range from 10 to 40°, while the scanning speed was 0.01°/min.

2.4.3. X-Ray Fluorescence. The chemical compositions of RM, RHA, and the prepared geopolymers were measured by XRF (ZSX Primus II; Rigaku Corp., Japan) to determine the difference in element content after the geopolymerization process.

2.4.4. Scanning Electron Microscope–Energy Dispersive X-Ray Spectroscopy. The surface morphologies of the samples were observed using a SEM (JSM-IT300, JEOL, Japan). Samples were coated with a thin layer of conducting material (gold) and imaged at various magnifications with an accelerating voltage of 10–15 kV. In addition, to observe the element distributions in the obtained geopolymers, an EDS (JSM-5300LV; JEOL Ltd., Japan) was also equipped.

2.4.5. Surface Area and Pore Properties. The BET surface area and the BJH pore size distribution of the obtained geopolymers were measured with a nitrogen gas adsorption instrument (TriStar II 3020; Micromeritics Instrument Corp., USA) at 77 K. The samples were dried at 60 °C for 24 h and evacuated under vacuum conditions before measurement.

2.4.6. Surface-Charged Determination. The change in surface charge of the geopolymers at different pH solutions was determined by a Zeta-potential analyzer (ELSE1NGK; Otsuka Electronics Co. Ltd., Japan). About 0.1 g of the geopolymer was placed in tubes containing 20 mL of KCl 0.1 M aqueous solution, followed by pH adjustment at 2, 4, 6, 8, 10, and 12 by NaOH 1 N NaOH and HCl 1 N HCl aqueous solution. The zeta potential values of the prepared geopolymers at different amounts of RHA were recorded at each specific pH, which was selected for the adsorption test.

https://doi.org/10.1021/acsomega.3c04691
ACS Omega 2023, 8, 41258–41272

Table 2. Mixture Proportions of Initial Materials, BET Surface Area, BJH Pore Volume, and Size of the Obtained Geopolymers

	mix proportion by weight (g per 100 g)							
sample	RM	RHA	Na_2SiO_3	NaOH 7 M	Si content (%)	surface area (m^2/g)	BJH pore volume (cm^3/g)	BJH pore size (nm)
RM					0.27	5.77	0.040	6.30
100RM0RHA	51	0	35	14	3.98	19.2	0.044	6.68
80RM20RHA	40.8	10.2	35	14	7.20	23.3	0.040	5.97
60RM40RHA	30.6	20.4	35	14	26.6	27.8	0.043	6.13
40RM60RHA	20.4	30.6	35	14	26.0	29.5	0.045	5.76
RHA					39.5	9.69	0.01	5.1

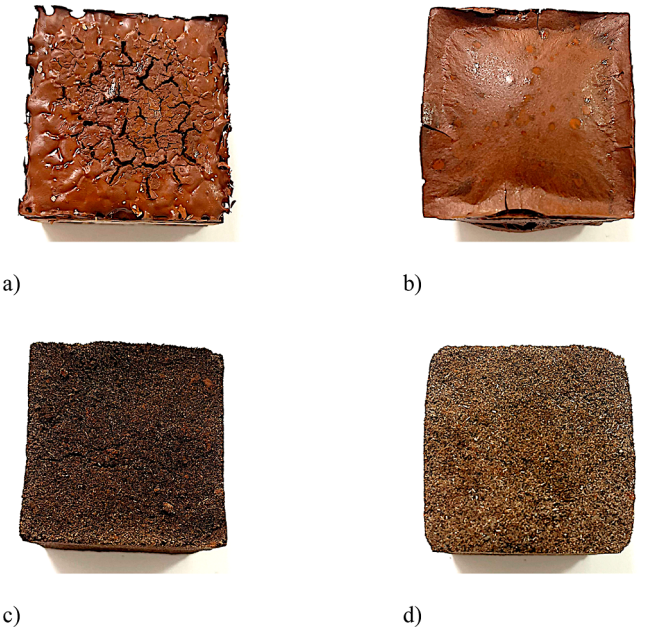

Figure 3. Images of the prepared geopolymers: (a) 100RM0RHA, (b) 80RM20RHA, (c) 60RM40RHA, and (d) 40RM60RHA.

2.5. Adsorption Experiment of MB. The stock dye solution of 1000 mg/L was prepared by directly dissolving MB in deionized water at pH 8. The adsorbent mass of the prepared geopolymer was 0.10 g and was placed in 20 mL of MB solutions from 20 to 120 mg/L. The mixtures were stirred for 180 min at 200 rpm and 273 K. After that, the sample was centrifuged at 3000 rpm for 10 min. The initial and residual concentrations were measured using a UV−vis spectrophotometer (V-750, Jasco, Japan) at a wavelength of 662 nm for MB. The removal efficiency of the geopolymers was measured using eq 1, and the adsorption capacity at any time q_t (mg/g) and adsorption capacity at equilibrium q_e (mg/g) were determined using eq 2.

The removal percentage (H %) was

$$H(\%) = \frac{C_0 - C_t}{C_0} \times 100 \quad (1)$$

where H was the removal capacity of the dyes adsorbed (%), and C_0 and C_t were the initial and time concentrations of dyes in the solution (mg/L), respectively.

The adsorption amount at the current time (q_t, mg/g) and equilibrium adsorption capacity (q_e, mg/g) were calculated according to the following equations

$$q_{t,e} = \frac{(C_0 - C_{t,e}) \times V}{M} \quad (2)$$

where C_0 and C_t (mg/L) were the concentrations of the solution at the initial time and time t (h), respectively, C_e (mg/L) was the equilibrium concentration of dye solution, V (L) was the volume of the contaminated solution, and m (g) was the weight of the dried adsorbent.

3. RESULTS AND DISCUSSION

3.1. Appearance of Geopolymers. The geopolymers prepared from RM in the presence of different RHA amounts from 0 to 60% are shown in Figure 3. It was observed that the

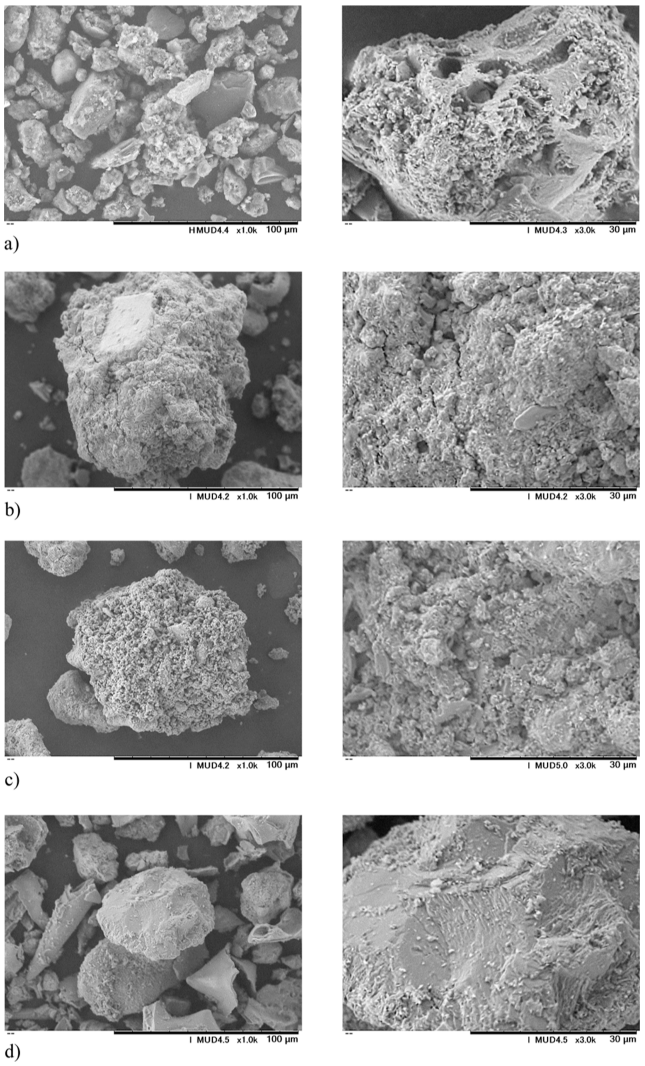

Figure 4. SEM images of (a) 100RM0RHA, (b) 80RM20RHA, (c) 60RM40RHA, and (d) 40RM60RHA at magnifications of 1000× (left) and 3000× (right).

https://doi.org/10.1021/acsomega.3c04691
ACS Omega 2023, 8, 41258−41272

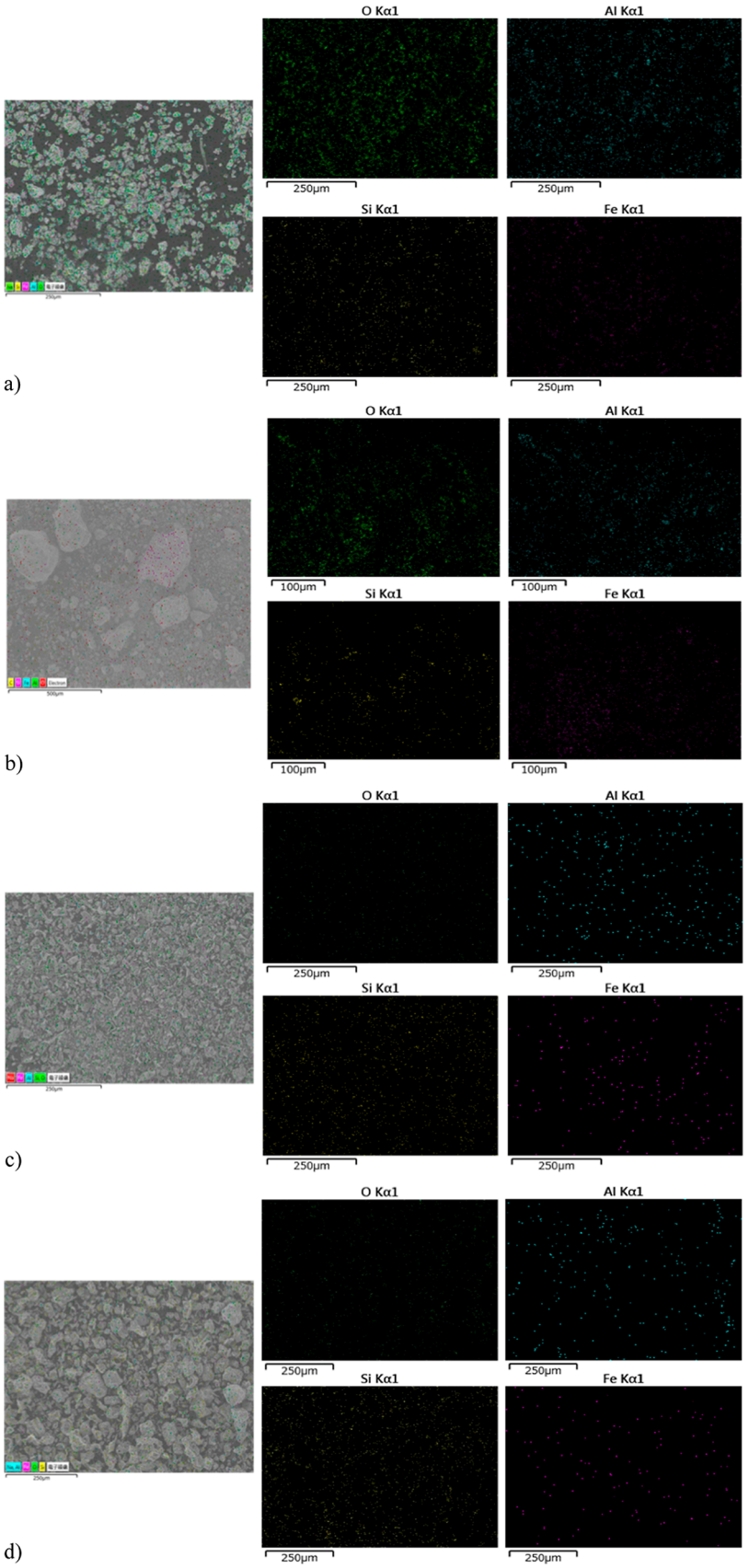

Figure 5. SEM−EDS mapping of (a) 100RM0RHA, (b) 80RM20RHA, (c) 60RM40RHA, and (d) 40RM60RHA.

color of the obtained geopolymers was attributed to the dose-dependence of RHA, which was gradually changed from dark orange for 0% to light brown for 60% of RHA. The geopolymer prepared from 100% RM was seen to have

https://doi.org/10.1021/acsomega.3c04691
ACS Omega 2023, 8, 41258−41272

Table 3. Main Element Content (%) from EDS Mapping

	main element content (%) from EDS mapping				
sample	Si	Al	Fe	O	Na
100RM0RHA	4.4	11.3	19.2	64.5	0.5
80RM20RHA	8.7	14.9	26.1	50.3	0.0
60RM40RHA	26.6	6.6	9.9	54.8	0.0
40RM60RHA	33.5	3.8	10.1	52.6	0.1

fractures on the surface due to the loss of water during the drying process. In the case of the mixed geopolymer, the distribution of RHA powder was observed, and the mass was much lighter compared to the RM-based geopolymer. As listed in Table 2, the Si content was changed between the initial materials, such as RM, RHA, and the fabricated geopolymers. The weight percentage of Si in the RM detected by XRF was 0.27%, while no significant difference was recorded in the cases of 60RM40RHA and 40RM60RHA at about 26%. However, at higher amounts of RHA, more than 60%, the geopolymer was unable to prepare because of the loss of mass balance in the compositions.

3.2. Properties of Geopolymers. *3.2.1. SEM Observation with EDS-Mapping Detection.* The morphological images of the prepared geopolymers at different amounts of RHA from 0 to 60% are illustrated in Figure 4. As seen, various shapes of 100RM0RHA particular matter were irregularly observed (Figure 4a). At a higher magnification of 3000×, the surface of the RM geopolymer was rougher due to the chemical interaction with the alkali activator, suggesting a phase transformation might have occurred. For the prepared geopolymers, such as 80RM20RHA (Figure 4b), the ash fillers were seen to be well-distributed on the surface of the geopolymer particles forming the dense outer structure. Similar results were observed in the case of the geopolymer having 40% RHA in the preparation. As seen in Figure 4c, the morphological structure of 60RM40RHA was more porous than the others. For the sample 40RM60RHA (Figure 4d), it was observed that the initial material seemed not to be influenced by the chemical reaction for the geopolymerization process. Apparently, there were several RHA tiny grains found on the surface of the RM particle, which suggests that the

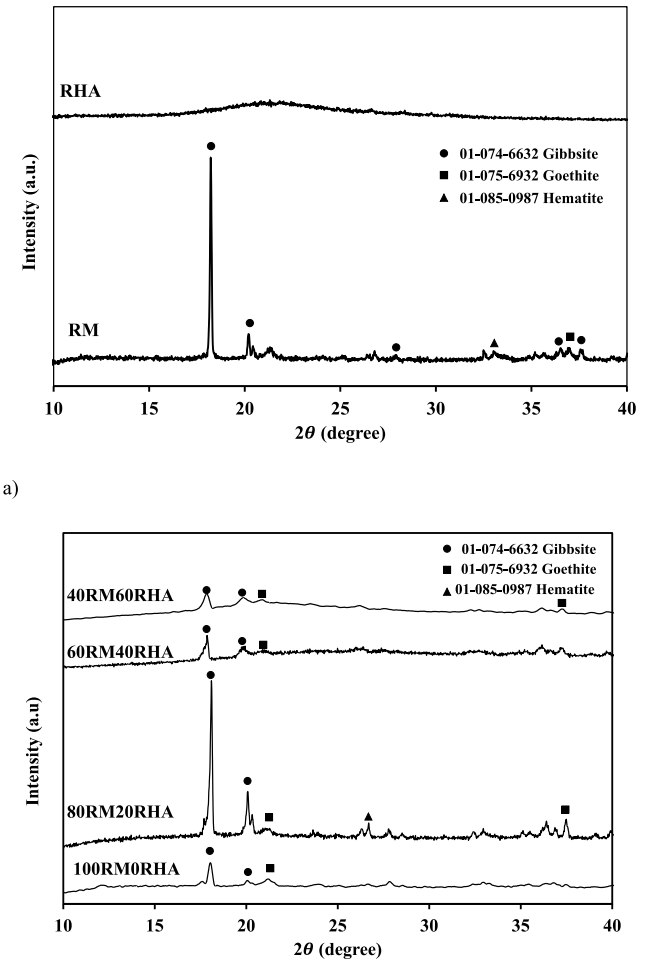

Figure 7. XRD pattern of RM, RHA (a), and the prepared geopolymers at different amounts of RHA (b).

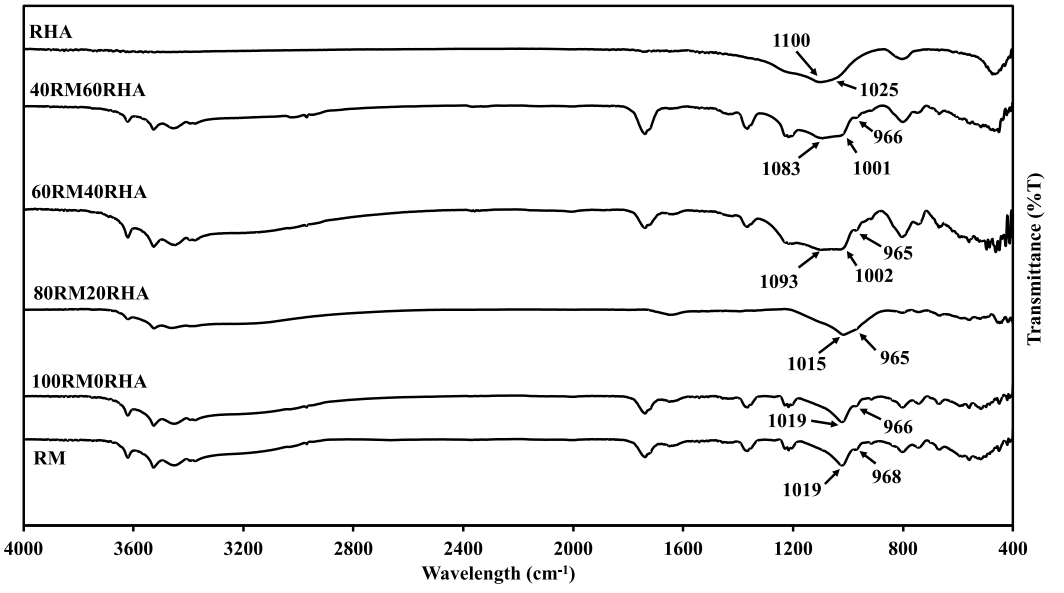

Figure 6. FT-IR spectrum of RM, RHA, and the prepared geopolymers at different amounts of RHA.

https://doi.org/10.1021/acsomega.3c04691
ACS Omega 2023, 8, 41258−41272

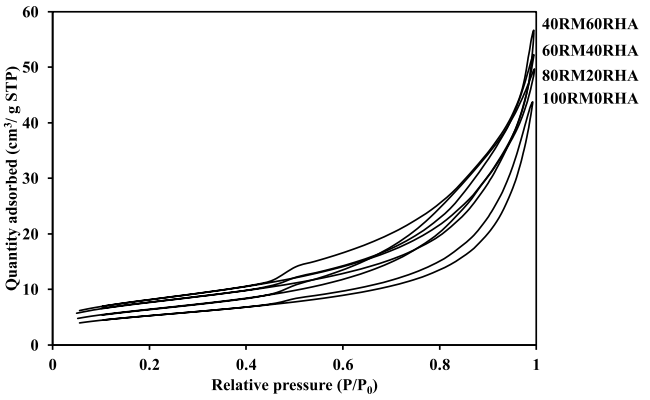

Figure 8. Nitrogen adsorption/desorption isotherm of the prepared geopolymers at different amounts of RHA.

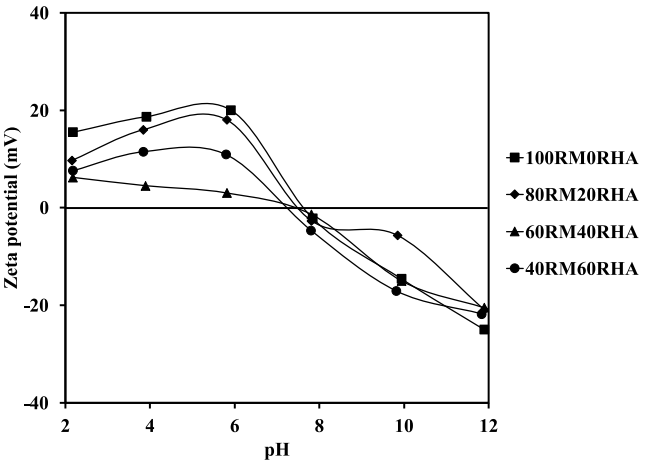

Figure 9. Zeta-potential of the prepared geopolymer at different amounts of RHA.

interaction between RM and the highly concentrated alkali solution was not well-conducted. This could be because when the RHA amount was up to 60% in the geopolymer composition, the strong additives seemed not to be able to interfere with the remaining portion of RM. Therefore, mostly the RM matters were maintained in the mixture, leading the surface somehow smoothly. This phenomenon could be similar to the study of Jian He et al.[52]

As illustrated in Figure 5a–g, the EDS mapping showed that the distribution of the elements in the prepared geopolymers was significantly different from the Si content due to the increased loading amount of RHA from 0 to 60% during the geopolymerization. The element composition detected by EDS is listed in Table 3. As listed, the content of Si element was increased from 4.4% for 100RM0RM to 33.5% for 40RM60RHA, suggesting that the RHA was dispersed in all of the geopolymer samples.

3.2.2. FT-IR Spectra. It has been known that potential interactions between chemicals through shifts in wavelengths or variations in the intensity of bands observed in the initial materials, such as RM, RHA, and prepared geopolymers with different compositions could be evaluated by FT-IR spectra. As seen in Figure 6, mostly in all the spectra of RM and the geopolymers, the hydroxyl-stretching band was presented in the region of 3450–3400 cm^{-1} wavelengths owing to the presence of hydrogen-bonded surface OH groups. The absorption peak near 3620 cm^{-1} was assigned to the inner-

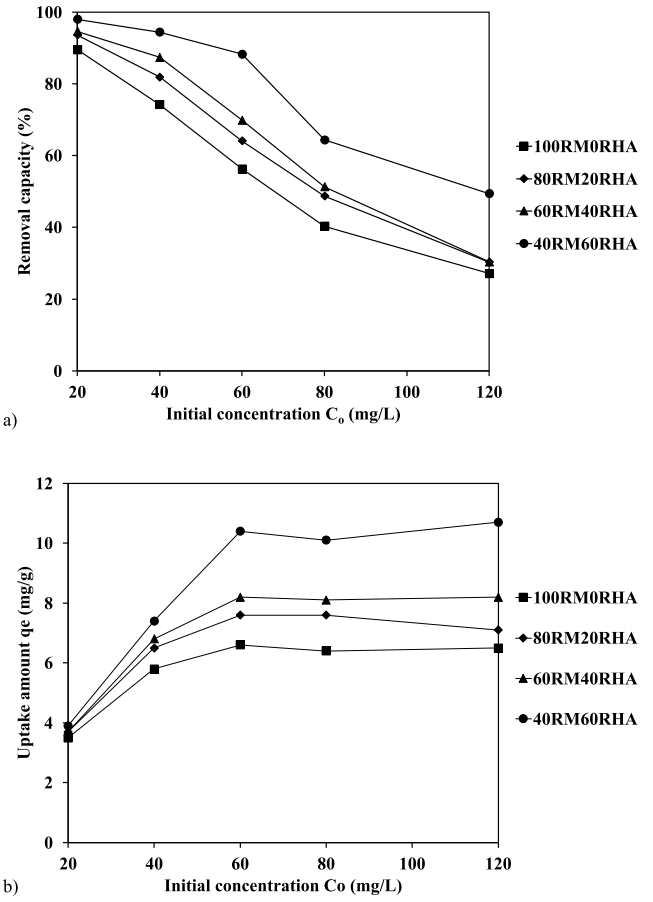

Figure 10. Removal capacity (a) and uptake amount (b) of prepared geopolymer at different initial concentrations of MB.

Table 4. Value of the Removal Capacity (%) and Uptake Amount (mg/g) of MB Adsorption of the Obtained Geopolymer at pH 8

sample	initial concentration Co (mg/L)	removal capacity (%)	uptake amount Qe (mg/g)
100RM0RHA	20	89.5	3.5
	40	74.2	5.8
	60	56.3	6.6
	80	40.3	6.4
	120	27.1	6.5
80RM20RHA	20	93.6	3.7
	40	81.9	6.5
	60	64.1	7.6
	80	48.7	7.6
	120	30.3	7.1
60RM40RHA	20	94.6	3.7
	40	87.4	6.8
	60	69.9	8.2
	80	51.3	8.1
	120	30.4	8.2
40RM60RHA	20	98	3.9
	40	94.4	7.4
	60	88.3	10.4
	80	64.4	10.1
	120	49.4	10.7

hydroxyl groups (Al_2OH dickite).[53] The band at the wavelength of 1736–1726 cm^{-1} represented the double

https://doi.org/10.1021/acsomega.3c04691
ACS Omega 2023, 8, 41258–41272

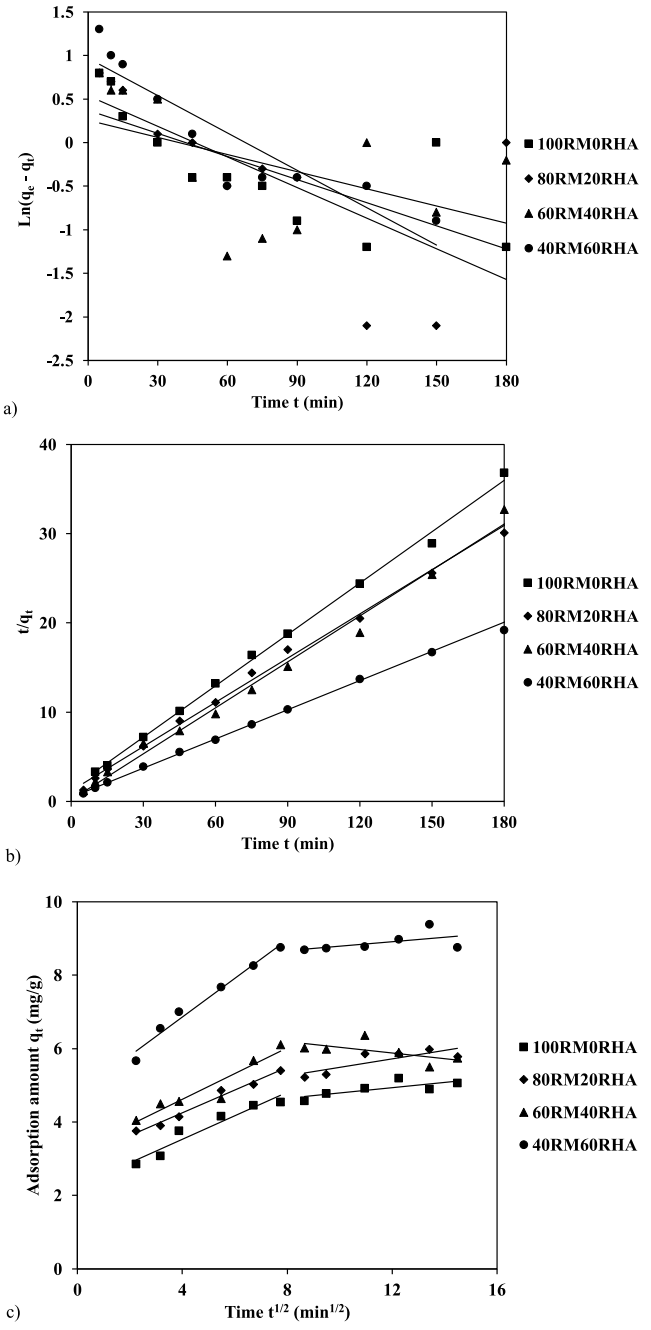

Figure 11. Linear form of pseudo-first-order (a), pseudo-second-order (b), and W−M (c) of the prepared geopolymer on the adsorption of MB.

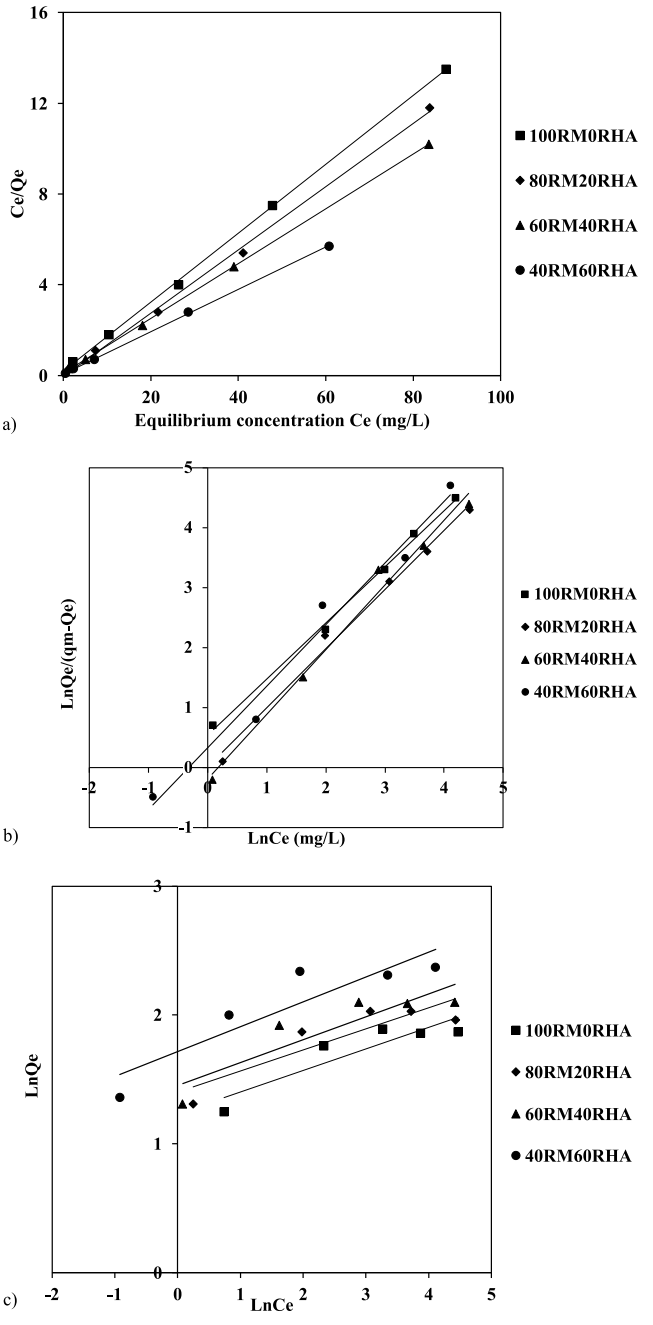

Figure 12. Linear isotherm of Langmuir (a), Sips (b), and Freundlich model (c) at different initial concentrations of MB.

bond of the C═O group, whereas the band detected at 1630 cm^{-1} was attributed to the bending vibration of H−O−H occluded inside the aluminosilicate structure.[54] The characteristic band of Si−O was also observed at 968 cm^{-1} in the case of RM. However, this wavelength was shifted to be lower at 966 and 965 cm^{-1} with added RHA during the geopolymerization.

Table 5. Kinetics Parameters for MB Adsorption on the Prepared Geopolymer

	PFO			PSO			W−M					
							k (mg/g·$min^{1/2}$)		C (mg/g)		R^2	
samples	q_e (mg/g)	k_1 (1/min)	R^2	q_e (mg/g)	k_2 (g/mg·min)	R^2	1st stage	2nd stage	1st stage	2nd stage	1st stage	2nd stage
100RM0RHA	1.45	0.0089	0.570	5.21	0.0369	0.998	0.32	0.06	2.25	4.07	0.979	0.569
80RM20RHA	1.72	0.0117	0.481	5.84	0.0293	0.998	0.31	0.08	3.03	4.32	0.898	0.670
60RM40RHA	1.29	0.0066	0.255	6.06	0.0273	0.994	0.35	0.07	3.21	6.82	0.980	0.376
40RM60RHA	2.63	0.0143	0.835	9.18	0.0118	0.997	0.53	0.07	4.75	8.18	0.928	0.266

https://doi.org/10.1021/acsomega.3c04691
ACS Omega 2023, 8, 41258−41272

Table 6. Isotherm Parameters of MB Adsorption by the Prepared Geopolymers at pH 8

	parameters								
	Langmuir			Sips			Freundlich		
sample	q_m (mg/g)	K_L (L/mg)	R^2	$1/n_S$	K_S (L/g)	R^2	$1/n$	K_F (L/g)	R^2
100RM0RHA	6.59	0.760	0.9996	0.936	1.721	0.9970	0.164	4.055	0.7764
80RM20RHA	7.17	1.022	0.9979	0.988	1.002	0.9908	0.167	3.439	0.8125
60RM40RHA	8.28	1.240	0.9998	1.081	0.821	0.9867	0.177	4.285	0.7978
40RM60RHA	10.74	1.180	0.9997	1.029	1.382	0.9781	0.193	5.568	0.8202

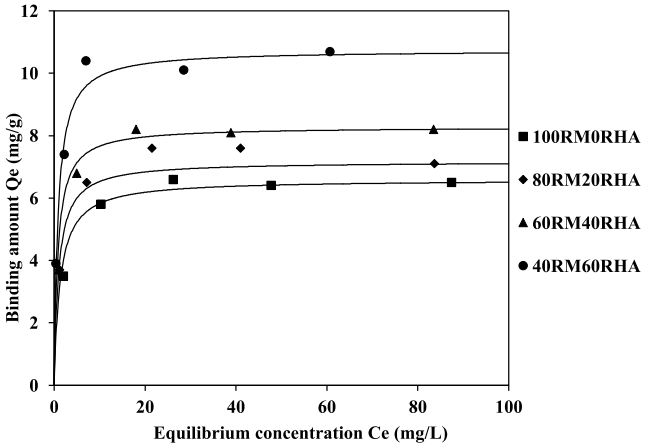

Figure 13. Adsorption isotherm of MB at different initial concentrations by the prepared geopolymers.

The position of the Si−O−T (T = Si or Al) asymmetric stretching band located at 1019 cm^{-1} was found to shift to the lower wavelength of 1015, 1002, and 1001 cm^{-1} when the RHA amount was added of 20, 40, and 60% in the geopolymer content, respectively.[53] Moreover, the band of O−Si−O/O−Al−O stretching at 1100 cm^{-1} in RHA was lightly shifted to 1083 and 1093 cm^{-1} in the case of 40RM60RHA and 60RM40RHA, respectively.[55,56] In addition, these peaks in the geopolymer structure seemed to broaden compared to those of RHA. This evidence suggested that the initial materials were well-interacted with the additives, and the formation of geopolymers between RM and RHA was confirmed.

3.2.3. XRD Pattern. The XRD analysis of RM, RHA, and the geopolymers prepared at different ratios of RM and RHA is shown in Figure 7. In the case of RM, crystalline phases such as goethite, hematite, and gibbsite were typically observed with different intensities (Figure 7a). There was no observation of silica oxide in the compounds of RM. As seen from that, gibbsite $Al(OH)_3$ was numerously found in the chemical composition of RM, whereas the amorphous phase of silica oxide was formed as the main component of RHA. It was observed that these crystalline phases were maintained with a shaft peak after the alkali activation (Figure 7b). As seen, no new crystalline phase occurred because the alkali activation was a reaction that involved and produced amorphous phases. However, the intensity of XRD patterns in the case of these prepared geopolymers was somehow lower than that of the initial RM.

3.2.4. BET Surface Area and BJH Determination. To evaluate the surface area and porosity of the obtained geopolymers, the N_2 gas adsorption isotherm was evaluated. Figure 8 depicts the adsorption−desorption process of N_2 gas under isothermal conditions when the relative pressure varied from 0.0 to 1.0. Based on that, it can be seen that all geopolymer materials tend to adsorb by type IV, in which the hysteresis loops are associated with the capillary condensation taking place in the mesoporous properties.[57] As seen, the BET surface values of the prepared geopolymers were improved compared to those of the initial materials, indicating that the interaction of RM and RHA with the activated alkali solution and binder occurred. When a higher mixed RHA content was added to the composition, the surface area of the geopolymer gradually increased. These results were found to be typically within the range reported.[58] With the increase of RHA from 0 to 60% in the prepared geopolymer, the surface area was enhanced from 19.2 m^2/g for 100RM0RHA to 29.5 m^2/g for 40RM60RHA. However, the excess amount of RHA up to 60% caused a reduction in the BJH pore size value. The SEM results indicated that the RM-based geopolymer having 60% RHA showed smooth materials with tiny grains on the surface, suspecting that the RHA powders tended to reduce the pore size of the obtained geopolymers, somehow leading to the deficiency interaction between the geopolymer compositions after the chemical process with NaOH activator and binder solution. As listed in Table 2, the Si content measured by XRF was constant at about 26%, while the RHA amount was increased from 40 to 60%, suggesting that the RHA fillers might be in agglomeration form at a high loading amount. These results indicated the pore size values of the obtained geopolymers could be influenced by the unequal distribution of RHA grains. As a consequence, the BJH pore size of the geopolymers decreased from 6.68 nm for 100RM0RHA to 5.76 nm for 40RM60RHA, respectively. Meanwhile, the BJH pore volume seemed to be unchanged at 0.044 cm^3/g and 0.045 cm^3/g for the samples prepared with 0 and 60% RHA. The values of BET surface area, pore size, and pore volume of RM, RHA, and the geopolymers are shown in Table 2.

3.2.5. Zeta Potential. Figure 9 shows the zeta potential as a function of pH of the different solutions of RM−RHA geopolymer powders. It has been known that the surface charge of RHA has negative values in a wide range of pHs, from 2 to 12.[58,59] Therefore, a higher amount of RHA was able to cause negative charges on the surface of the mixed geopolymer powders. It is found that the zeta potentials of the sample are highly negative in the pH range between 7 and 12. For this reason, MB ions were disassociated in an aqueous solution, which existed as positively charged ions. Therefore, an increase in OH^- concentration at high pH could improve MB adsorption based on the electrostatic attraction.[60]

3.2.6. Dye Adsorption. pH was almost considered one of the most critical parameters in determining the influence of the testing environment on the adsorption capacity of the material. It was known that high concentrations of H^+ ions were at low pH. Hence, these H^+ ions formed in the aqueous solution were able to compete with other MB cations on the adsorption binding sites. Consequently, the interaction that took place was electrostatic repulsion, reducing the adsorption capacity of MB

https://doi.org/10.1021/acsomega.3c04691
ACS Omega 2023, 8, 41258−41272

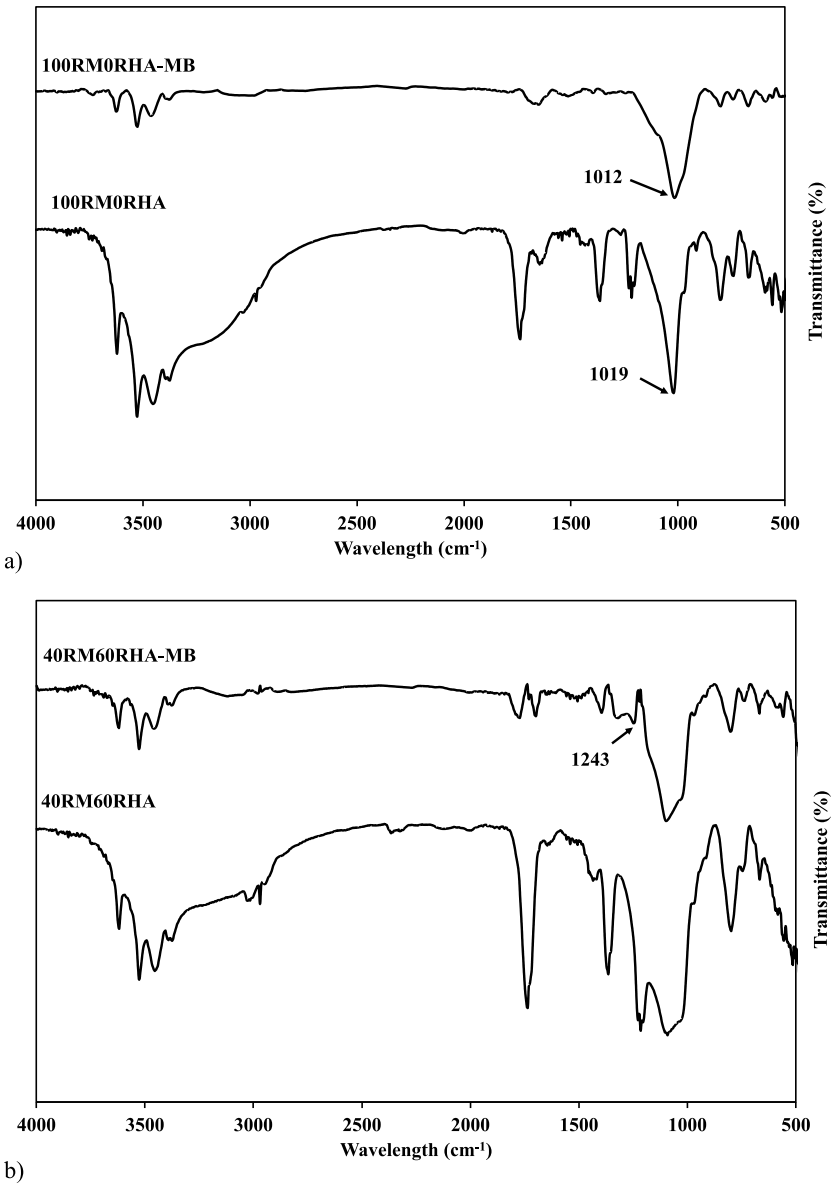

Figure 14. FT-IR spectrum of 100RM0RHA (a) and 40RM60RHA (b) before and after the adsorption of MB.

on the surface of the material. In contrast, a negatively charged surface of the adsorbent was formed in a high-pH solution due to the presence of OH^- groups in the aqueous solution. Therefore, an increase in the adsorption capacity of the geopolymers with MB ions was expected, which was based on electrostatic attraction between them. The zeta potential results indicated that the surface charge of the prepared geopolymer composites might be negative at pH 8, which was strongly considered to perform the MB adsorption test. In this study, pH 8 was selected because this value was close to neutral, which was not considered for pH adjustment in practical applications. The effect of initial concentration on the percentage removal of MB by the geopolymer powders is shown in Figure 10. As seen, the removal efficiency was higher than 80% of all samples when the initial concentration of MB was applied at 20 mg/L (Figure 10a). Apparently, when the initial concentrations of MB were changed from 40 to 120, the removal capacities of all samples gradually decreased. As is known, higher MB concentrations could restrict the number of adsorption sites in the geopolymer composites, leading to a decrease in the removal percentage. Therefore, sufficient adsorption sites remained for the sorption of MB ions at lower initial concentrations of the MB solutions.

Herein, the removal capacity was tested for the 100RM0RHA, 80RM20RHA, 60RM40RHA, and 40RM60RHA, where RHA contented at 0, 20, 40, and 60%, respectively. The removal capacities were gradually increased at a higher loading of the RHA content in the geopolymer composite. The reason might be because the sorption sites of RHA in the composite occurred, as seen in the results of surface area and pore size values. When the initial concentration of MB was 40 mg/L, the value of the percentage removal increased from 74.2% for 100RM0RHA and 94.4% for 40RM60RHA, respectively. However, the removal efficiency was reduced to 27.1 and 49.4% for the geopolymer composites with 0 and 60% RHA when the concentration of MB was 120 mg/L. As seen in Figure 10b, the initial concentration of MB had a strong effect on the binding amount of MB on the prepared geopolymers with different mixing ratios of RHA. A similar tendency was recorded when the concentration was

https://doi.org/10.1021/acsomega.3c04691
ACS Omega 2023, 8, 41258−41272

Scheme 1. Proposed Adsorption Mechanism of RM-Based Geopolymer (a) and RM-Based Geopolymer with Different Amounts of RHA (b)

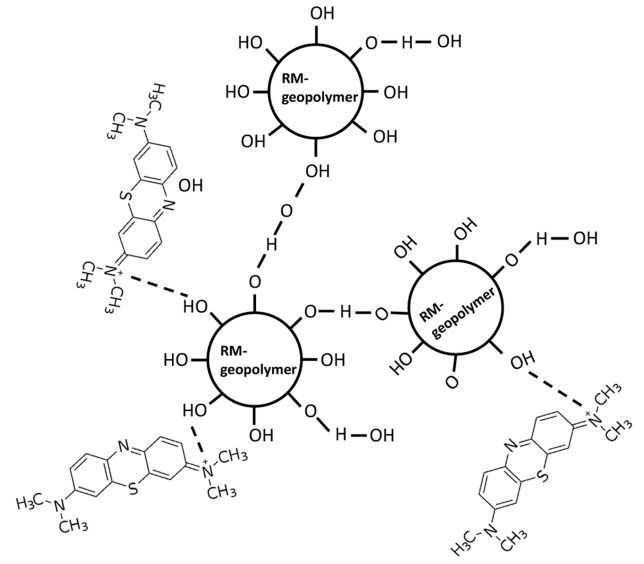

a)

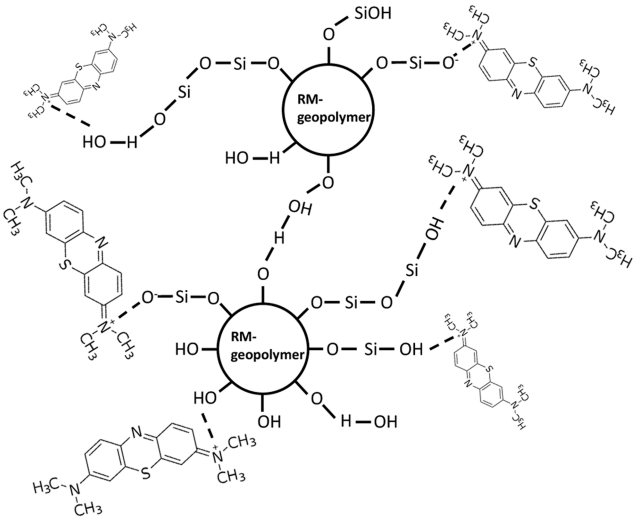

b)

increased from 20 to 60 mg/L. However, when the initial concentration of MB was up to 120 mg/L, the uptake amount seemed to be relatively constant in the case of 40RM60RHA. These results indicated that higher MB initial solutions may be refused by the adsorption sties in geopolymer structures. In addition, there was a slight decrease in the adsorption capacity of MB when the mixing amounts of RHA in the RM-based geopolymers ranged from 0 to 40%. The percentage removal of MB and the uptake amount are concluded in Table 4.

In order to evaluate the effect of contact time on the adsorption rate of MB by the prepared geopolymer, the pseudo-first-order (PFO), pseudo-second-order (PSO), and Weber–Morris (W–M) equations were applied to clarify the adsorption kinetics. The linear forms of PFO (eq 3), PSO (eq 4), and W–M (eq 5) are shown below

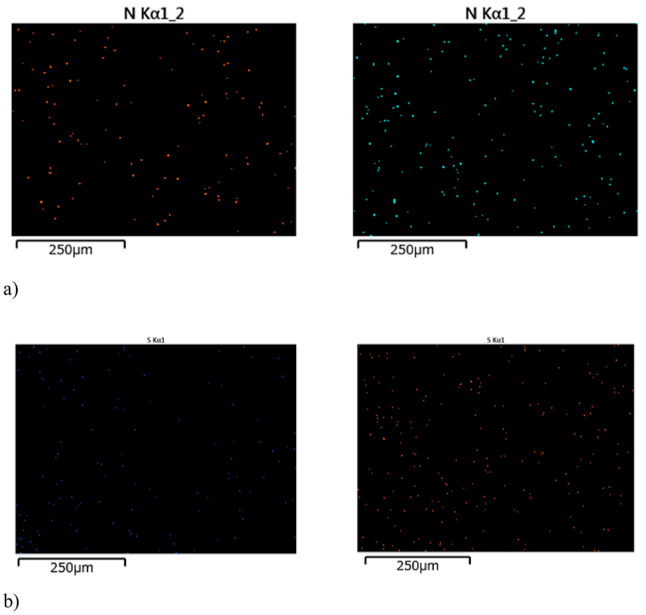

Figure 15. Distribution of Nitrogen (left) and Sulfur (right) in SEM–EDS images of (a) 100RM0RHA and (b) 40RM60RHA after MB-adsorption at 120 mg/L after 3 h at pH 8.

Table 7. Comparison of MB-Adsorption Capacity of Other Geopolymer-Based Adsorbents

sample	adsorption capacity (mg/g)	references
Kaolin-based geopolymer	4.6–7.64	64,65
Phosphoric acid-activated metakaolin-based geopolymer	4.26	66
monolithic geopolymer −50% expanded glass composites	4.9	67
red-mud-based geopolymer	6.59	this study
red-mud and 60% rice-husk-ash-based geopolymer	10.74	this study

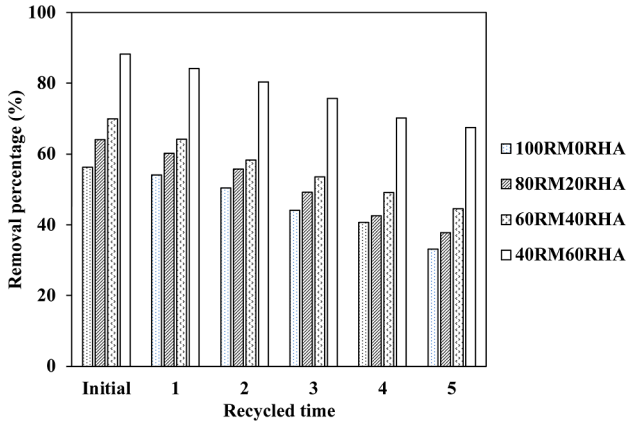

Figure 16. Regeneration of the MB-loaded geopolymer composite-based adsorbent.

$$\mathrm{Ln}(q_e - q_t) = -k_1 t + \ln q_e \quad (3)$$

$$\frac{1}{q_t} = \frac{1}{K_2 q_e^2} + \frac{t}{q_e} \quad (4)$$

$$q_t = kt^{0.5} + C \quad (5)$$

https://doi.org/10.1021/acsomega.3c04691
ACS Omega 2023, 8, 41258−41272

where q_e and q_t are the adsorption capacity at equilibrium and at time t (min), respectively. k_1 (1/min) and k_2 (g/mg·min) are the rate constants for PFO and PSO, k (mg/g·min$^{1/2}$) is the intraparticle diffusion constant, and C (mg/g) is a constant to the related boundary layer thickness for the W−M adsorption.

The linear form of PFO and PSO of the prepared geopolymer composite as a function of contact time is listed in Figure 11. As seen from the results, the adsorption amount of MB on the RM−RHA geopolymer composite gradually increased when immersed at a higher contacting time, up to 180 min. The fitting results of the experimental data for MB were better fitted with the PSO mode, in which the R^2 reached 0.998 for 100RM0RHA and 0.997 for 40RM60RHA. Therefore, the adsorption mechanism might also involve the chemisorption between the MB ion and the prepared geopolymer.[61] However, the PFO and the PSO models were not able to identify the diffusion mechanism of adsorbents. Essentially, the adsorption process of porous adsorbents possesses three stages: (i) contaminant transfer from the solution to the adsorbent surface by a liquid boundary film, (ii) contaminant transfer from the adsorbent surface to the intraparticle active sites, and (iii) interactions of the contaminant molecules with the available sites on both the external and internal surfaces of the adsorbent.[62] Thus, the Weber−Morris equation was utilized to further analyze the rate-controlling mechanism in the adsorption process. According to the Weber−Morris model, if the adsorption process involved intraparticle diffusion, the relationship between q_t and $t^{0.5}$ is a straight line. Figure 11c shows the plots of MB uptake vs $t^{1/2}$ for the prepared geopolymer composite at different loading amounts of RHA. The results were related by two straight lines, indicating that two steps were strongly suggested: the first one was assumed to be mass transfer, and the second was intraparticle diffusion.[63] In the first stage, the film diffusion stage, the k constant of the geopolymer composite toward the MB ion was faster at higher content of RHA in the geopolymer composition. It has been observed at 0.32 mg/g·min$^{1/2}$ for 100RM0RHA and 0.53 mg/g·min$^{1/2}$ for 40RM60RHA, respectively.

The second linear segment was slower compared to the first linear segment and could be attributed to the intraparticle diffusion stage, which was seen at a lower k constant. In addition, the C constant related to the boundary layer thickness was greater in both stages for the samples having RHA loadings and increased gradually with the content of RHA for both stages. Moreover, the values of R^2 in the case of the first stage were higher and closer to 1 than those of the second stage. Therefore, RHA could be effective in enhancing the MB-adsorption capacity of the RM-based geopolymer. Table 5 summarizes the kinetics parameters for the MB-adsorption by the prepared geopolymers.

The Langmuir and Freundlich models were used to propose the relationship between the residual concentration of dye in solution and the adsorption capacity of geopolymers at a constant temperature. The linear equation of the Langmuir isotherm model was used as in eq 6 below

$$\frac{C_e}{q_e} = \frac{1}{K_L q_m} + \frac{C_e}{q_m} \tag{6}$$

where q_m (mg/g) is the maximum adsorption capacity, and K_L (L/mg) is the Langmuir constant.

The linear equation of the Sips model is shown in eq 7

$$\ln\left(\frac{q_e}{q_m - q_e}\right) = \frac{1}{n_S}\ln C_e + \ln K_S \tag{7}$$

where K_S (L/g) and n_S are the Sips isotherm constants related to the adsorption capacity and to the adsorption strength, respectively.

In the case of the Freundlich isotherm model, the linear equation was presented as eq 8 follows

$$\ln q_e = \ln K_F + \frac{1}{n_F}\ln C_e \tag{8}$$

where K_F (L/g) and n_F are the Freundlich isotherm constants related to the adsorption capacity and to the adsorption strength, respectively.

The influence of the initial concentrations was relatively carried out with the Langmuir and Freundlich isotherm models. Based on the linear coefficients of these equations, we can determine how the adsorption of the RM−RHA geopolymer composites took place. From the results of the MB adsorption amount of RM−RHA geopolymers on the effect of the initial concentration of MB, the adsorption isotherm was plotted to determine the parameters of the two models. As seen from the linearity of the plots in Figure 12a, the R^2 was about 0.999 for all samples, which were almost close to one. It meant that the adsorption isotherms of MB obeyed the Langmuir model. Therefore, the Langmuir isotherm model better fitted the experimental results, which meant that the adsorption of MB onto the RM−RHA geopolymer composites was monolayer adsorption, and the adsorption was at specific homogeneous sites within the adsorbent. In the case of the Sips model, a reduction in R^2 values obtained from all samples was observed compared to those of the Langmuir model (Figure 12b). Otherwise, the lowest value of R^2 obtained in the Freundlich model was 0.7764 for 100RM0RHA and 0.8202 for 40RM60RHA, respectively (Figure 12c). The parameter values of the adsorption isotherm are listed in Table 6. It was seen that the binding amount of the MB ion on 40RM60RHA was higher than that of others in the adsorption test. Figure 13 shows the adsorption isotherm of MB by the prepared geopolymer at various amounts of RHA. For instance, when the RHA contents were increased from 0 to 60%, the maximum binding amount of MB increased to 6.59 and 10.74 mg/g, respectively. This result suggested that RHA was able to be a potential additive to enhance the adsorption capacity of RM-based geopolymers. It has been observed that the chemisorption occurred during the adsorption of MB by the RM−RHA geopolymer composite. Therefore, FT-IR measurement was used to evaluate the difference before and after the adsorption of MB in an aqueous solution. As seen in Figure 14a, in the case of the sample 100RM0RHA after being immersed in the MB aqueous solution at 60 mg/L of initial concentration, the peak observed at 1019 cm^{-1} relating to the Si−O−Ti bonding was shifted to a lower wavelength of 1012 cm^{-1} obtained in the 100RM0RHA-MB. Thus, the chemical interaction between the RM-based geopolymer and the MB ion was confirmed. However, the presence of MB in the RM-based geopolymer was not well indicated due to the low adsorption amount. For the geopolymer composite having 60% RHA contents, the peak representing C−N bonding was seen at 1243 cm^{-1} for 40RM60RHA-MB (Figure 14b). In addition, no significant peak shifting occurred in the case of

https://doi.org/10.1021/acsomega.3c04691
ACS Omega 2023, 8, 41258−41272

40RM60RHA before and after the MB adsorption, suggesting the electrostatic forces formed by the negatively charged silica oxide, the main component of RHA, and the MB cationic ion. The proposed mechanisms in the case of individual RM-based geopolymers and RM−RHA-mixed geopolymers for the adsorption of MB ions are illustrated in Scheme 1. It could be easily suspected that the main interaction between RM-based geopolymers and MB cationic ions was electrostatic attraction due to the negatively charged group of silanon on the surface of geopolymer powders. However, it was supposed that these geopolymer powders could interact with each other because of the hydrated formation while dispersing in an aqueous solution (Scheme 1a). When RHA was mixed at different amounts from 0 to 60%, its main component, silica oxide, might play an important role in the higher adsorption of the MB ion, as seen in Scheme 1b. Therefore, the uptake performance was enhanced in the presence of RHA in the RM-geopolymer structure.

In addition, the SEM−EDS images of the samples 100RM0RHA and 40RM60RHA suggested that the better distributions of nitrogen and sulfur elements were observed in the geopolymer having higher a RHA content (Figure 15). Therefore, the uptake performance was enhanced in the presence of RHA mixed into the structure of the RM-based geopolymer.

The adsorption capacity between various adsorbents for the removal of MB in aqueous solutions is presented in Table 7. Compared to other geopolymers, RM−RHA geopolymers were suitable sorbents for dye removal from aqueous media. Because of the low content of silica oxide, the industrial byproduct with a large amount of RM was not effectively used to generate geopolymers. Therefore, most of the geopolymers from coal fly ash or others showed an extremely higher adsorption amount of MB than RM-based geopolymers. Despite the fact that there is a problem due to the large amount of this waste, this study would like to bring a potential application for these materials to reduce the environmental impact, decrease the treatment cost, and enhance their economic value. Additionally, the combination of two different wastes toward a promising symbiosis of industrial and agricultural waste and an enhancement in awareness that waste is a precious resource have been successfully presented in this study.

3.3. Regeneration of MB-Loaded Geopolymer Composite-Based Adsorbent. The reusability of the MB-load geopolymer composite was tested to measure the recycling properties of these adsorbents. The MB-loaded samples were desorbed by immersion in 0.1 N HCl aqueous solution for 24 h to obtain the saturated releasing concentration of MB from the adsorbent. After that, these samples were centrifuged at 3000 rpm for 10 min and dried at 80 °C for 24 h. The results indicated that the removal percentage of MB in aqueous solution by the geopolymer composite decreased after five consecutive recycles. As seen in Figure 16, all the samples exhibited a good adsorption of MB, which was above 50% at initial concentration of 60 mg/L for the second round. The removal efficiency decreased gradually with the loading amount of RHA in the RM-based geopolymer. For the fourth time, when the addition of RHA was 40 to 60%, the relative geopolymer composite still maintained the uptake performance around 50% for 60RM40RHA and up to 70.2% for 40RM60RHA, respectively. Only the sample with the highest content of RHA at 60% was seen to well retain MB ions after the fifth recycle. This occurrence was due to the reduced availability of active sites within the composite adsorbent or material loss.[68] The adsorption sites inside the materials gradually became saturated, resulting in an equilibrium of dye adsorption.[69] From this experiment, the RHA was proven to be a potential waste-based inorganic filler for maintaining the regeneration of the RM-based geopolymer.

4. CONCLUSIONS

RM-based geopolymers with various mixing amounts of RHA were successfully prepared in the presence of activators such as NaOH 7 M and Na_2SiO_3 aqueous solution at a curing temperature of 60 °C for 24 h. The increment in RHA-loading amount in the geopolymer composition from 0 to 60% improved the Si content to 3.98% for 100RM0RHA and 26.0% for 40RM60RHA, following the increment in surface area values of 19.2 and 29.5 m^2/g and reduction in the pore size observation, respectively. In the MB adsorption experiment at pH 8, the results showed that a higher amount of RHA in the geopolymer composition enhanced the adsorption capacity within 180 min. In addition, the adsorption behavior of the mixed geopolymer for MB was in good agreement with the Langmuir model, suggesting that adsorption occurred on the homogeneous monolayer surface. The addition of RHA to the geopolymer might increased the adsorption site toward MB molecules. From this study, RHA could be a useful filler to improve the uptake performance of RM-based adsorbents used in wastewater treatment. Especially at the present study, the RHA in this study was not on the analytical grade; however, the addition of this agro-waste-derived material in RM-based geopolymer showed an effective increment in dye removal in wastewater. Therefore, waste or byproducts from industrial activities and agriculture such as RM and RHA, should be strongly considered to be a naturally alternative adsorbent toward sustainable development. For application as an attractive, low-cost dye filter, a pilot experiment should also be conducted to compare the differences between experimental and practical conditions.

AUTHOR INFORMATION

Corresponding Authors

Khoa Dang Nguyen − *Faculty of Environment, Van Lang University, Ho Chi Minh City 70000, Vietnam;* orcid.org/0000-0001-8831-989X; Email: khoa.nd@vlu.edu.vn

Noor Haida Mohd Kaus − *School of Chemical Sciences, Universiti Sains Malaysia, Penang 11800, Malaysia;* Email: noorhaida@usm.my

Authors

Trang Tran Thu − *Faculty of Environment, Van Lang University, Ho Chi Minh City 70000, Vietnam*

Anh Thi Hoang Tran − *Faculty of Environment, Van Lang University, Ho Chi Minh City 70000, Vietnam*

Oanh Thi Kim Le − *Faculty of Environment, Van Lang University, Ho Chi Minh City 70000, Vietnam*

Suresh Sagadevan − *Nanotechnology and Catalysis Research Centre, Universiti Malaya, Kuala Lumpur 50603, Malaysia*

Complete contact information is available at: https://pubs.acs.org/10.1021/acsomega.3c04691

https://doi.org/10.1021/acsomega.3c04691
ACS Omega 2023, 8, 41258−41272

Author Contributions

K.D.N.: conceptualization, methodology, formal analysis, data curation, visualization, and original draft preparation. T.T.T.: data curation and reviewing and editing. A.T.H.T.: data curation, visualization, and validation. O.T.K.L.: formal analysis, data curation, and visualization. S.S.: reviewing and editing. H.M.K.: conceptualization, visualization, and reviewing and editing.

Notes

The authors declare no competing financial interest.

■ ACKNOWLEDGMENTS

The authors would like to extend their heartfelt appreciation to all the members in the experimental laboratory of the Faculty of Environment, Van Lang University, for their invaluable assistance throughout the entire research process. Their support has been instrumental in the successful completion of this study. Furthermore, the authors confirm that this research did not receive any specific grants from funding agencies in the public, commercial, or not-for-profit sectors.

■ REFERENCES

(1) Farhana, K.; Kadirgama, K.; Mahamude, A. S. F.; Mica, M. T. Energy consumption, environmental impact, and implementation of renewable energy resources in global textile industries: an overview towards circularity and sustainability. *Mater. Circ. Econ.* **2022**, *4* (1), 15.

(2) Berradi, M.; Hsissou, R.; Khudhair, M.; Assouag, M.; Cherkaoui, O.; El Bachiri, A.; El Harfi, A. Textile finishing dyes and their impact on aquatic environs. *Heliyon* **2019**, *5* (11), No. e02711.

(3) Liu, Q. Pollution and Treatment of Dye Waste-Water. *IOP Conf.* **2020**, *514* (5), 052001.

(4) Zhu, C.; Feng, Q.; Ma, H.; Wu, M.; Wang, D.; Wang, Z. Effect of Methylene Blue on the Properties and Microbial Community of Anaerobic Granular Sludge. *BioResources* **2018**, *13* (3), 6033−6046.

(5) Xiao, J.; Lv, W.; Xie, Z.; Tan, Y.; Song, Y.; Zheng, Q. Environmentally friendly reduced graphene oxide as a broad-spectrum adsorbent for anionic and cationic dyes via π-π interactions. *J. Mater. Chem. A* **2016**, *4* (31), 12126−12135.

(6) Fadillah, G.; Saleh, T. A.; Wahyuningsih, S.; Ninda Karlina Putri, E.; Febrianastuti, S. Electrochemical removal of methylene blue using alginate-modified graphene adsorbents. *Chem. Eng. J.* **2019**, *378*, 122140.

(7) Sakin Omer, O.; Hussein, M. A.; Hussein, B. H. M.; Mgaidi, A. Adsorption thermodynamics of cationic dyes (methylene blue and crystal violet) to a natural clay mineral from aqueous solution between 293.15 and 323.15 K. *Arabian J. Chem.* **2018**, *11* (5), 615−623.

(8) Dai, Y.; Zhang, N.; Xing, C.; Cui, Q.; Sun, Q. The adsorption, regeneration and engineering applications of biochar for removal organic pollutants: A review. *Chemosphere* **2019**, *223*, 12−27.

(9) Mechi, N.; Ben Khemis, I.; Dotto, G. L.; Franco, D.; Sellaoui, L.; Ben Lamine, A. Investigation of the adsorption mechanism of methylene blue (MB) on Cortaderia selloana flower spikes (FSs) and on Cortaderia selloana flower spikes derived carbon fibers (CFs). *J. Mol. Liq.* **2019**, *280*, 268−273.

(10) Sadegh, H.; Ali, G. A. M. Potential Applications of Nanomaterials in Wastewater Treatment: Nanoadsorbents Performance Hussain, A., Ahmed, S., Eds.; IGI Global: Hershey, PA, USA, 2019, pp 51−61.*Advanced Treatment Techniques for Industrial Wastewater*

(11) Jain, A. K.; Gupta, V. K.; Bhatnagar, A.; Suhas. Utilization of industrial waste products as adsorbents for the removal of dyes. *J. Hazard. Mater.* **2003**, *101* (1), 31−42.

(12) Sud, D.; Mahajan, G.; Kaur, M. P. Agricultural waste material as potential adsorbent for sequestering heavy metal ions from aqueous solutions - A review. *Bioresour. Technol.* **2008**, *99* (14), 6017−6027.

(13) Sulyman, M.; Namiesnik, J.; Gierak, A. Low-cost Adsorbents Derived from Agricultural By-products/Wastes for Enhancing Contaminant Uptakes from Wastewater: A Review. *Polym. J. Environ. Stud.* **2017**, *26* (2), 479−510.

(14) Davidovits, J. Geopolymers. *J. Therm. Anal.* **1991**, *37* (8), 1633−1656.

(15) Davidovits, J. Properties of geopolymer cements. *First international conference on alkaline cements and concretes*; Kiev State Technical University Kiev: Ukraine, 1994, pp 131−149.

(16) Onutai, S.; Jiemsirilers, S.; Thavorniti, P.; Kobayashi, T. Aluminium hydroxide waste based geopolymer composed of fly ash for sustainable cement materials. *Constr. Build. Mater.* **2015**, *101*, 298−308.

(17) Pinto, L. F.; Montaño, A. M.; González, C. P.; Barón, G. C. Removal of rhodamine B in wastewater from the textile industry using geopolymeric material. *J. Phys.: Conf. Ser.* **2019**, *1386* (1), 012040.

(18) Novais, R. M.; Carvalheiras, J.; Tobaldi, D. M.; Seabra, M. P.; Pullar, R. C.; Labrincha, J. A. Synthesis of porous biomass fly ash-based geopolymer spheres for efficient removal of methylene blue from wastewaters. *J. Cleaner Prod.* **2019**, *207*, 350−362.

(19) Maleki, A.; Mohammad, M.; Emdadi, Z.; Asim, N.; Azizi, M.; Safaei, J. Adsorbent materials based on a geopolymer paste for dye removal from aqueous solutions. *Arabian J. Chem.* **2020**, *13* (1), 3017−3025.

(20) Rasaki, S. A.; Bingxue, Z.; Guarecuco, R.; Thomas, T.; Minghui, Y. Geopolymer for use in heavy metals adsorption, and advanced oxidative processes: A critical review. *J. Cleaner Prod.* **2019**, *213*, 42−58.

(21) Cheng, T. W.; Lee, M. L.; Ko, M. S.; Ueng, T. H.; Yang, S. F. The heavy metal adsorption characteristics on metakaolin-based geopolymer. *Appl. Clay Sci.* **2012**, *56*, 90−96.

(22) Medri, V.; Papa, E.; Mor, M.; Vaccari, A.; Natali Murri, A.; Piotte, L.; Melandri, C.; Landi, E. Mechanical strength and cationic dye adsorption ability of metakaolin-based geopolymer spheres. *Appl. Clay Sci.* **2020**, *193*, 105678.

(23) Suwan, T. Categories and Types of Raw Materials Using in Geopolymer Cement Production: An Overview. *Solid State Phenom.* **2018**, *280*, 481−486.

(24) Pimraksa, K.; Chindaprasirt, P.; Rungchet, A.; Sagoe-Crentsil, K.; Sato, T. Lightweight geopolymer made of highly porous siliceous materials with various Na2O/Al2O3 and SiO2/Al2O3 ratios. *J. Mater. Sci. Eng. A* **2011**, *528* (21), 6616−6623.

(25) Onutai, S.; Jiemsirilers, S.; Wada, S.; Thavorniti, P. Effect of sodium hydroxide solution on the properties of geopolymer based on fly ash and aluminium waste blend. *Suranaree J. Sci. Technol.* **2014**, *21* (1), 9.

(26) Görhan, G.; Kürklü, G. The influence of the NaOH solution on the properties of the fly ash-based geopolymer mortar cured at different temperatures. *Composites, Part B* **2014**, *58*, 371−377.

(27) Yao, X.; Zhang, Z.; Zhu, H.; Chen, Y. Geopolymerization process of alkali-metakaolinite characterized by isothermal calorimetry. *Thermochim. Acta* **2009**, *493* (1−2), 49−54.

(28) Nazari, A.; Bagheri, A.; Riahi, S. Properties of geopolymer with seeded fly ash and rice husk bark ash. *J. Mater. Sci. Eng. A* **2011**, *528* (24), 7395−7401.

(29) USGS. *Mineral commodity summaries 2020*; USGS: Reston, VA, 2020, p 204.

(30) Sutar, H.; Mishra, S.; Sahoo, S.; Chakraverty, A. P.; Maharana, H. Progress of Red Mud Utilization: An Overview. *Am. Chem. Sci. J.* **2014**, *4*, 255−279.

(31) Lemougna, P. N.; Wang, K.-t.; Tang, Q.; Cui, X.-m. Synthesis and characterization of low temperature (<800°C) ceramics from red mud geopolymer precursor. *Constr. Build. Mater.* **2017**, *131*, 564−573.

(32) Ribeiro, D.; Labrincha, J. A.; Morelli, M. Effect of red mud addition on the corrosion parameters of reinforced concrete evaluated

https://doi.org/10.1021/acsomega.3c04691
ACS Omega 2023, 8, 41258−41272

by electrochemical methods. *Rev. IBRACON Estrut. Mater.* **2012**, *5*, 451−467.
(33) Joseph, C. G.; Yap, Y. H. T.; Krishnan, V.; Puma, G. L. Application of modified red mud in environmentally-benign applications: A review. *Environ. Eng. Res.* **2020**, *25*, 795.
(34) Hairi, S. N. M.; Jameson, G. N. L.; Rogers, J. J.; MacKenzie, K. J. D. Synthesis and properties of inorganic polymers (geopolymers) derived from Bayer process residue (red mud) and bauxite. *J. Mater. Sci.* **2015**, *50* (23), 7713−7724.
(35) Liu, Y.; Naidu, R.; Ming, H.; Dharmarajan, R.; Du, J. Effects of thermal treatments on the characterisation and utilisation of red mud with sawdust additive. *Waste Manage. Res.* **2016**, *34* (6), 518−526.
(36) Ahmed, S.; Meng, T.; Taha, M. Utilization of red mud for producing a high strength binder by composition optimization and nano strengthening. *Nanotechnol. Rev.* **2020**, *9* (1), 396−409.
(37) Gräfe, M.; Power, G.; Klauber, C. Bauxite residue issues: III. Alkalinity and associated chemistry. *Hydrometallurgy* **2011**, *108* (1−2), 60−79.
(38) Khale, D.; Chaudhary, R. Mechanism of geopolymerization and factors influencing its development: a review. *J. Mater. Sci.* **2007**, *42* (3), 729−746.
(39) Hajjaji, W.; Andrejkovičová, S.; Zanelli, C.; Alshaaer, M.; Dondi, M.; Labrincha, J. A.; Rocha, F. Composition and technological properties of geopolymers based on metakaolin and red mud. *Mater. Des.* **2013**, *52*, 648−654.
(40) Duxson, P.; Mallicoat, S. W.; Lukey, G. C.; Kriven, W. M.; van Deventer, J. S. J. The effect of alkali and Si/Al ratio on the development of mechanical properties of metakaolin-based geopolymers. *Colloids Surf., A* **2007**, *292* (1), 8−20.
(41) Bakar, R. A.; Yahya, R.; Gan, S. N. Production of High Purity Amorphous Silica from Rice Husk. *Procedia Chem.* **2016**, *19*, 189−195.
(42) Prasad, R.; Pandey, M. Rice Husk Ash as a Renewable Source for the Production of Value Added Silica Gel and its Application: An Overview. *Bull. Chem. React. Eng. Catal.* **2012**, *7*, 1−25.
(43) Dang, N.; Nguyen, T.; Phan, T. D.; Tran, H.; Dang, P. V.; Nguyen, H. Q. Synthesis of silica nanoparticles from rice husk ash. *Sci. Technol. Dev. J.* **2018**, *20*, 50−54.
(44) Wang, S.; Li, H. Structure directed reversible adsorption of organic dye on mesoporous silica in aqueous solution. *Microporous Mesoporous Mater.* **2006**, *97* (1−3), 21−26.
(45) Nilchi, A.; Janitabar-Darzi, S.; Rasouli-Garmarodi, S. Sol-Gel Preparation of Nanoscale TiO₂/SiO₂ Composite for Eliminating of Con Red Azo Dye. *Mater. Sci. Appl.* **2011**, *02* (05), 476−480.
(46) Chen, J.; Liu, X.; Li, G.; Nie, X.; An, T.; Zhang, S.; Zhao, H. Synthesis and characterization of novel SiO2 and TiO2 co-pillared montmorillonite composite for adsorption and photocatalytic degradation of hydrophobic organic pollutants in water. *Catal. Today* **2011**, *164* (1), 364−369.
(47) Shaghayeghi Toosi, F.; Hosseiny, M.; Joghataei, A.; Shaghayeghi Toosi, F. The Application of Sio2 Nanoparticles for Anionic Dye Removal from Aqueous Solution. *Arch. Hyg. Sci.* **2017**, *6* (2), 136−144.
(48) Nikolić, I.; Janković-Častvan, I.; Krivokapić, J.; Djurovic, D.; Radmilovic, V.; Radmilović, V. Geopolymerization of low-grade bauxite. *Mater. Tehnol.* **2014**, *48*, 39.
(49) Ye, N.; Yang, J.; Ke, X.; Zhu, J.; Li, Y.; Xiang, C.; Wang, H.; Li, L.; Xiao, B. Synthesis and characterization of geopolymer from Bayer red mud with thermal pretreatment. *J. Am. Ceram. Soc.* **2014**, *97* (5), 1652−1660.
(50) He, J.; Jie, Y.; Zhang, J.; Yu, Y.; Zhang, G. Synthesis and characterization of red mud and rice husk ash-based geopolymer composites. *Cem. Concr. Compos.* **2013**, *37*, 108−118.
(51) Hu, Y.; Liang, S.; Yang, J.; Chen, Y.; Ye, N.; Ke, Y.; Tao, S.; Xiao, K.; Hu, J.; Hou, H.; Fan, W.; Zhu, S.; Zhang, Y.; Xiao, B. Role of Fe species in geopolymer synthesized from alkali-thermal pretreated Fe-rich Bayer red mud. *Constr. Build. Mater.* **2019**, *200*, 398−407.
(52) He, J.; Jie, Y.; Zhang, J.; Yu, Y.; Zhang, G. Synthesis and characterization of red mud and rice husk ash-based geopolymer composites. *Cem. Concr. Compos.* **2013**, *37*, 108−118.
(53) Perná, I.; Hanzlíček, T.; Šupová, M. The identification of geopolymer affinity in specific cases of clay materials. *Appl. Clay Sci.* **2014**, *102*, 213−219.
(54) Singh, S.; Aswath, M. U.; Das Biswas, R.; Ranganath, R. V.; Choudhary, H. K.; Kumar, R.; Sahoo, B. Role of iron in the enhanced reactivity of pulverized Red mud: Analysis by Mössbauer spectroscopy and FTIR spectroscopy. *Case Stud. Constr. Mater.* **2019**, *11*, No. e00266.
(55) Mohd Basri, M. S. A. U. M. F. M. N. I. M. R. T. I. R. H. A.-B. G. B. C. S. O. C. F. S. M.; Mustapha, F.; Mazlan, N.; Ishak, M. R. Rice husk ash-based geopolymer binder: Compressive strength, optimize composition, FTIR spectroscopy, microstructural, and potential as fire-retardant material. *Polymers* **2021**, *13*, 4373.
(56) Adams, F. V.; Ikotun, B. D.; Patrick, D. O.; Mulaba-Bafubiandi, A. F. Characterization of Rice Hull Ash and Its Performance in Turbidity Removal From Water. *Part. Sci. Technol.* **2014**, *32* (4), 329−333.
(57) Thommes, M.; Kaneko, K.; Neimark, A. V.; Olivier, J. P.; Rodriguez-Reinoso, F.; Rouquerol, J.; Sing, K. S. W. Physisorption of gases, with special reference to the evaluation of surface area and pore size distribution (IUPAC Technical Report). *Pure Appl. Chem.* **2015**, *87* (9−10), 1051−1069.
(58) Gutierrez, A. M.; Hotza, D.; Dutra, G. B.; Nogueira, A. L.; Franco, C. V.; Acchar, W.; Rambo, C. R. Rice Husk Ash Impregnated with Silver Nanoparticles for Water Purification. *Mater. Sci. Forum* **2014**, *798*−*799*, 727−731.
(59) Zhang, Z.; He, W.; Zheng, J.; Wang, G.; Ji, J. Rice Husk Ash-Derived Silica Nanofluids: Synthesis and Stability Study. *Nanoscale Res. Lett.* **2016**, *11* (1), 502.
(60) Liou, T.-H.; Liou, Y. H. Utilization of Rice Husk Ash in the Preparation of Graphene-Oxide-Based Mesoporous Nanocomposites with Excellent Adsorption Performance. *Materials* **2021**, *14*, 1214.
(61) Ge, Y.; Cui, X.; Kong, Y.; Li, Z.; He, Y.; Zhou, Q. Porous geopolymeric spheres for removal of Cu(II) from aqueous solution: Synthesis and evaluation. *J. Hazard. Mater.* **2015**, *283*, 244−251.
(62) Hui, K. S.; Chao, C. Y. H.; Kot, S. C. Removal of mixed heavy metal ions in wastewater by zeolite 4A and residual products from recycled coal fly ash. *J. Hazard. Mater.* **2005**, *127* (1−3), 89−101.
(63) Belhachemi, M.; Belala, Z.; Lahcene, D.; Addoun, F. Adsorption of phenol and dye from aqueous solution using chemically modified date pits activated carbons. *Desalin. Water Treat.* **2009**, *7* (1−3), 182−190.
(64) Jin, H.; Zhang, Y.; Wang, Q.; Chang, Q.; Li, C. Rapid removal of methylene blue and nickel ions and adsorption/desorption mechanism based on geopolymer adsorbent. *Colloid Interface Sci. Commun.* **2021**, *45*, 100551.
(65) Yousef, R. I.; El-Eswed, B.; Alshaaer, M.; Khalili, F.; Khoury, H. The influence of using Jordanian natural zeolite on the adsorption, physical, and mechanical properties of geopolymers products. *J. Hazard. Mater.* **2009**, *165* (1−3), 379−387.
(66) Khan, M. I.; Min, T. K.; Azizli, K.; Sufian, S.; Ullah, H.; Man, Z. Effective removal of methylene blue from water using phosphoric acid based geopolymers: synthesis, characterizations and adsorption studies. *RSC Adv.* **2015**, *5* (75), 61410−61420.
(67) Rożek, P.; Król, M.; Mozgawa, W. Lightweight geopolymer-expanded glass composites for removal of methylene blue from aqueous solutions. *Ceram. Int.* **2020**, *46* (12), 19785−19791.
(68) Sayğili, H.; Güzel, F. Effective removal of tetracycline from aqueous solution using activated carbon prepared from tomato (Lycopersicon esculentum Mill.) industrial processing waste. *Ecotoxicol. Environ. Saf.* **2016**, *131*, 22−29.
(69) Ma, M.; Chen, Y.; Zhao, X.; Tan, F.; Wang, Y.; Cao, Y.; Cai, W. Effective removal of cation dyes from aqueous solution using robust cellulose sponge. *J. Saudi Chem. Soc.* **2020**, *24*, 915−924.

https://doi.org/10.1021/acsomega.3c04691
ACS Omega 2023, 8, 41258−41272